JACS
JOURNAL OF THE AMERICAN CHEMICAL SOCIETY

Subscriber access provided by American Chemical Society

Article

Epitaxial Heterostructures: Side-to-Side Si–ZnS, Si–ZnSe Biaxial Nanowires, and Sandwichlike ZnS–Si–ZnS Triaxial Nanowires

Junqing Hu, Yoshio Bando, Zongwen Liu, Takashi Sekiguchi, Dmitri Golberg, and Jinhua Zhan

J. Am. Chem. Soc., **2003**, 125 (37), 11306-11313• DOI: 10.1021/ja030235l • Publication Date (Web): 22 August 2003

Downloaded from http://pubs.acs.org on March 29, 2009

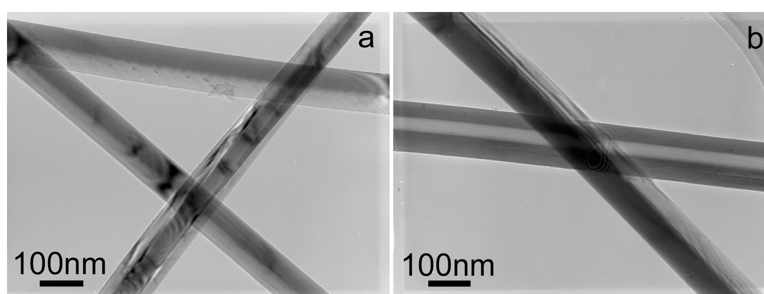

More About This Article

Additional resources and features associated with this article are available within the HTML version:

- Supporting Information
- Links to the 18 articles that cite this article, as of the time of this article download
- Access to high resolution figures
- Links to articles and content related to this article
- Copyright permission to reproduce figures and/or text from this article

View the Full Text HTML

ACS Publications
High quality. High impact.

Journal of the American Chemical Society is published by the American Chemical Society. 1155 Sixteenth Street N.W., Washington, DC 20036

J|A|C|S
ARTICLES
Published on Web 08/22/2003

Epitaxial Heterostructures: Side-to-Side Si−ZnS, Si−ZnSe Biaxial Nanowires, and Sandwichlike ZnS−Si−ZnS Triaxial Nanowires

Junqing Hu,* Yoshio Bando, Zongwen Liu, Takashi Sekiguchi, Dmitri Golberg, and Jinhua Zhan

Contribution from the Advanced Materials Laboratory and Nanomaterials Laboratory, National Institute for Materials Science, Namiki 1-1, Tsukuba, Ibaraki 305-0044, Japan

Received April 15, 2003; E-mail: HU.Junqing@nims.go.jp

Abstract: Epitaxial semiconducting heterostructures: side-to-side Si−ZnS, Si−ZnSe biaxial nanowires, and sandwichlike ZnS−Si−ZnS triaxial nanowires were grown via a simple two-stage thermal evaporation of mixed SiO and ZnS or SiO and ZnSe powders under a precise temperature control. Each nanowire had a uniform diameter of 40−120 nm and length ranging from several to several tens of micrometers. Subnanowires of Si, ZnS, and ZnSe within them had a diameter of 20−50, 40−60, and 20−50 nm, respectively. The optical property (nanoscale cathodoluminescence) was also investigated from these new structures. It is proposed that the Si nanowires formed through disproportionation of SiO to Si in the first evaporation stage and then served as one-dimensional nanoscale substrates (or templates) for an epitaxial growth of ZnS or ZnSe nanowires in the following thermal evaporation of ZnS or ZnSe powders. The present results suggest that the simple method might be useful for the synthesis of many other heterostructures containing Si and II−VI or III−V semiconducting composite nanowires to meet the growing demands of nanoscale science and technology.

Introduction

One-dimensional nanostructures having heterojunctions are of particular interest with respect to potential applications in nanoelectronics and nanophotonics.[1] Diverse functions have been realized by assembling two semiconducting nanowires or nanotubes into crossed junctions.[2−6] Recently, novel axial semiconductor nanowire heterostructures (supperlattices) with composition modulation have been prepared from GaAs/GaP and Si/SiGe nanowires,[7−11] and it has been demonstrated that they may have highly promising applications ranging from nanobarcodes to polarized nanoscale light-emitting diodes. If one-dimensional heterostructures with a well-defined compositional profile along the wire radial direction can be realized within semiconductor nanowires, new nanoelectronic devices, such as nanowaveguide and nanocapcipator, might be obtained. So far, a bilayer TiO_2/SnO_2 nanotape (or a composite nanoribbon) has been obtained through an epitaxial growth of TiO_2 on a SnO_2 nanoribbon (as a substrate) via a pulsed laser deposition.[12] In a related study, Si−Ge core−shell coaxial nanowire heterostructures have been grown by modulating the composition of the reactant gases in a process of chemical vapor deposition method.[13] However, the reported bilayer nanoribbons and core−shell nanowire heterostructures were made of analogous direct semiconductors (TiO_2 and SnO_2)[12] or indirect semiconductors (Si and Ge).[13] ZnS and ZnSe, well-known wide direct band-gap (∼3.68 eV for ZnS, ∼2.7 eV for ZnSe) II−VI semiconductors, have been considered as the most promising materials for fabrication of blue electroluminescent (EL)[14,15] diodes and blue-green light-emitting devices,[16,17] respectively. One-dimensional Si nanowires in particular are potentially very attractive, given the central role in the semiconductor industry and hence the existing set of known fabrication technologies.[18] It is known that the bulk quantity of Si nanowires has been

(1) Sze, S. M. *Physics of Semiconductor Devices*; Wiley-Interscience: New York, 1981.
(2) Hu, J. T.; Ouyang, M.; Yang, P. D.; Lieber, C. M. *Nature* **1999**, *399*, 48−51.
(3) Cui, Y.; Lieber, C. M. *Science* **2001**, *291*, 851−853.
(4) Cui, Y.; Wei, Q. Q.; Park, H. K.; Lieber, C. M. *Science* **2001**, *293*, 1289−1292.
(5) Duan, X. F.; Huang, Y.; Cui, Y.; Wang, J. E.; Lieber, C. M. *Nature* **2001**, *409*, 66−69.
(6) Huang, Y.; Duan, X. F.; Cui, Y.; Lauhon, L. J.; Kim, K. H.; Lieber, C. M. *Science* **2001**, *294*, 1313−1317.
(7) Lieber, C. M. *Nano Lett.* **2002**, *2*, 81−82.
(8) Björk, B. T.; Ohlsson, B. J.; Sass, T.; Persson, A. I.; Thelander, C.; Magnusson, M. H.; Deppert, K.; Wallenberg, L. R.; Samuelson, L. *Appl. Phys. Lett.* **2002**, *80*, 1058−1060.
(9) Björk, M. T.; Ohlsson, B. J.; Sass, T.; Persson, A. I.; Thelander, C.; Magnusson, K.; Deppert, M. H.; Wallenberg, L. R.; Samuelson, L. *Nano Lett.* **2002**, *2*, 87.
(10) Gudiksen, M. S.; Lauhon, L. J.; Wang, J.; Smith, D. C.; Lieber, C. M. *Nature* **2002**, *415*, 617−620.
(11) Wu, Y.; Fan, R.; Yang, P. *Nano Lett.* **2002**, *2*, 83−86.
(12) He, R.; Law, M.; Fan, R.; Kim, F.; Yang, P. *Nano Lett.* **2002**, *2*, 1109−1112.
(13) Lauhon, L. J.; Gudiksen, M. S.; Wang, D. L.; Lieber, C. M. *Nature* **2002**, *420*, 57−61.
(14) Thioulouse, P. *J. Cryst. Growth* **1985**, *72*, 545−552.
(15) Nakano, R.; Matsumoto, H.; Endo, T.; Shimada, J.; Sakagami, N.; Miura, N. *Jpn. J. Appl. Phys.* **1988**, *27*, L2103−L2104.
(16) Haase, M. A.; Qiu, J.; Depuydt, J. M.; Cheng, H. *Appl. Phys. Lett.* **1991**, *59*, 1272−1274.
(17) Xie, W.; Grillo, D. C.; Gunshor, R. L.; Kobayashi, M.; Hua, G. C.; Otsuka, N. *Appl. Phys. Lett.* **1992**, *60*, 463−465.
(18) Ma, D. D. D.; Lee, C. S.; Au, F. C. K.; Tong, S. Y.; Lee, S. T. *Science* **2003**, *299*, 1874−1877.

10.1021/ja030235l CCC: $25.00 © 2003 American Chemical Society

grown by the disproportionation of SiO powder at elevated temperature.[19−21] In this study, we try to use Si nanowires as one-dimensional nanoscale substrates for an epitaxial growth of ZnS or ZnSe nanowires. Our synthesis is based on a simple catalyst-free thermal evaporation of mixture of SiO and ZnS or SiO and ZnSe powders via a two-stage careful temperature-controlled process. In this process, Si nanowires were first formed from the disproportionation of SiO powder, and ZnS or ZnSe nanowires were then grown on the Si nanowire substrates via a thermal evaporation of ZnS or ZnSe powder. The resulting products are side-to-side Si−ZnS, Si−ZnSe biaxial nanowires, and ZnS−Si−ZnS triaxial nanowires, which consist of two sides or three layers of subnanowires of Si, ZnS, and ZnSe.

Experimental Section

The growth of side-to-side Si−ZnS, Si−ZnSe biaxial nanowires, and ZnS−Si−ZnS triaxial nanowires in the present work has been achieved in a vertical induction furnace, as described in detail elsewhere.[22,23] Briefly, the furnace consists of a fused-quartz tube (50 cm in length, 12 cm in outer diameter, and 0.25 cm in wall thickness) and an induction-heated cylinder (30 cm in length, 4.5 cm in outer diameter, and 3.5 cm in inner diameter) made of high-purity graphite coated with a C fiber thermo-insulating layer. The inductively heated cylinder had one inlet thin C pipe and outlet thin C pipe on its top and base, respectively. A graphite crucible containing a mixed powder of SiO (1.0 g, −325 mech, Sigma-Aldrich) and ZnS (1.5 g, 99.99%, Sigma-Aldrich) or SiO (1.0 g) and ZnSe (1.5 g, 99.99%, Sigma-Aldrich) was placed at the center cylinder zone, where the temperature was monitored with an optical pyrometer with an estimated accuracy of ±10 °C. After evacuation of the quartz tube to a pressure of ∼1−2 Torr, a carrier high-purity Ar (99.99%) gas was introduced into the tube at a flow rate of 80 sccm (standard cubic centimeter per minute) and at ambient pressure. The mixed SiO and ZnS powders or mixed SiO and ZnSe powders were rapidly heated to and maintained at 1300 °C for 1 h and then further heated to 1600 or 1500 °C for 1.5 h. After the reaction was terminated and the furnace was cooled to the room temperature, the resulting product was collected and characterized using an X-ray powder diffractometer (XRD, RINT 2200) with Cu Kα radiation, scanning electron microscopy (SEM, JSM-6700F), transmission electron microscopy (TEM, JEM-3100FFF, equipped with a field emission-type electron gun and Ω-type energy filter) with an X-ray energy dispersive spectrometer (EDS). Two different types of samples were prepared for the TEM characterization: one is the regular sample prepared by conventional dispersing followed by carbon film fishing, so that the nanowires were held by the carbon films for transfer to the microscope, and the other is a cross-sectional sample. Details of the sample preparation can be found elsewhere.[24] The cathodoluminescence (CL) spectroscopy and imaging were carried out using a high spatial resolution (∼50 nm) and a low-energy CL (HRLE-CL) system and a thermal field emission scanning electron microscope (TFE-SEM, Hitachi S4200).

Results and Discussion

Thermal evaporation of the mixed SiO and ZnS powders under a two-stage temperature control resulted in pale-brown

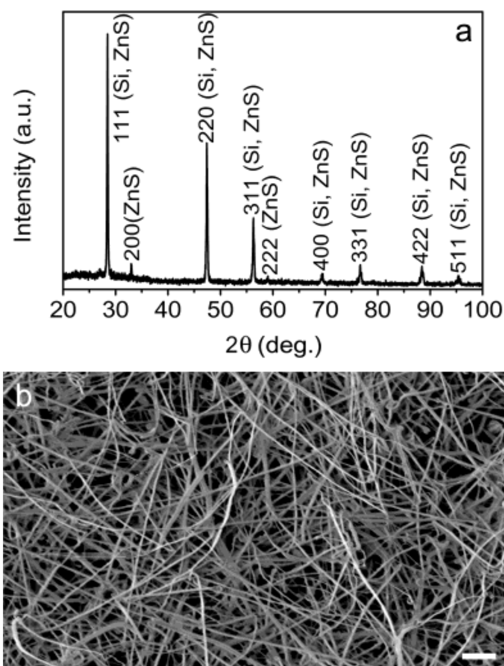

Figure 1. (a) XRD pattern recorded from the product obtained from thermal evaporation of a mixed powder of SiO and ZnS. (b) SEM image of the as-grown product. Scale bar: 1 μm.

products grown on the C fiber thermo-insulating layer. The yield of the product was estimated to be ∼2−3%, according to the amount of SiO powder used. XRD pattern (Figure 1a) shows that the as-grown product is a composite material containing diamond-cubic Si (JCPDS file: 27-1402) and a zinc blende (cubic) form of ZnS (JCPDS file: 05-0566). No characteristic peaks from other crystalline forms are detected in the XRD pattern. SEM observation (Figure 1b) reveals that the as-prepared product consists of a great quantity of wirelike nanostructures with typical lengths in the range of several to several tens of micrometers. These nanowires are randomly oriented, and most of them are relatively straight, but some of them are curved. Taken together, the XRD and SEM results indicate that the as-grown product is a composite material of Si and ZnS with wirelike morphology. Detailed microstructures of the product will be further investigated using TEM, HRTEM, electron diffraction (ED), and EDS.

Low-magnification TEM images are shown in Figure 2, a and b. The clear variation in contrast along the length suggests that the grown product appears to display two side-to-side biaxial (Figure 2a) and three-layer sandwichlike triaxial (Figure 2b) nanowire structures that are distinct from the recently reported core−shell nanowire structures.[13] The tip-end natures (Figure 2, c and d) of the composite nanowires further demonstrate that the geometries of side-to-side and sandwichlike structures are well maintained throughout their entire lengths. EDS nanoanalysis reveals that the light-contrast layer is pure Si, whereas the dark-contrast layer (or layers) is composed of ZnS (shown below). Each side-to-side biaxial and sandwichlike triaxial nanowire structure has a uniform diameter along its whole length. The typical diameter of these composite structures ranges from 60 to 120 nm, and the diameters of Si- and ZnS-side subnanowires within them are ∼30−40 and ∼40−60 nm, respectively. Importantly, from the cross-sectional TEM images of the as-grown nanowires, the elliptic cross-sectional shapes

(19) Wang, N., Tang, Y. H.; Zhang, Y. F.; Lee, C. S.; Lee, S. T. *Phys. Rev. B* **1998**, *58*, R16024−R16026.
(20) Lee, S. T.; Zhang, Y. F.; Wang, N.; Tang, Y. H.; Bello, I.; Lee, C. S. *J. Mater. Res.* **1999**, *14*, 4503−4507.
(21) Shi, W. S.; Peng, H. Y.; Xu, L.; Wang, N.; Tang, Y. H.; Lee, S. T. *Adv. Mater*. **2000**, *12*, 1927−1930.
(22) Golberg, D.; Bando, Y.; Bourgeois, L.; Kurashima, K.; Sato, T. *Carbon* **2000**, *38*, 2017−2027.
(23) Han, W. Q.; Bando, Y.; Kurashima, K.; Sato, T. *Appl. Phys. Lett.* **1998**, *73*, 3085−3087−3089.
(24) Tadanori, Y.; Masahiro, K.; Motoi, K.; Koji, N.; Makoto, S. *J. Electron Microsc.* **1995**, *44*, 488.

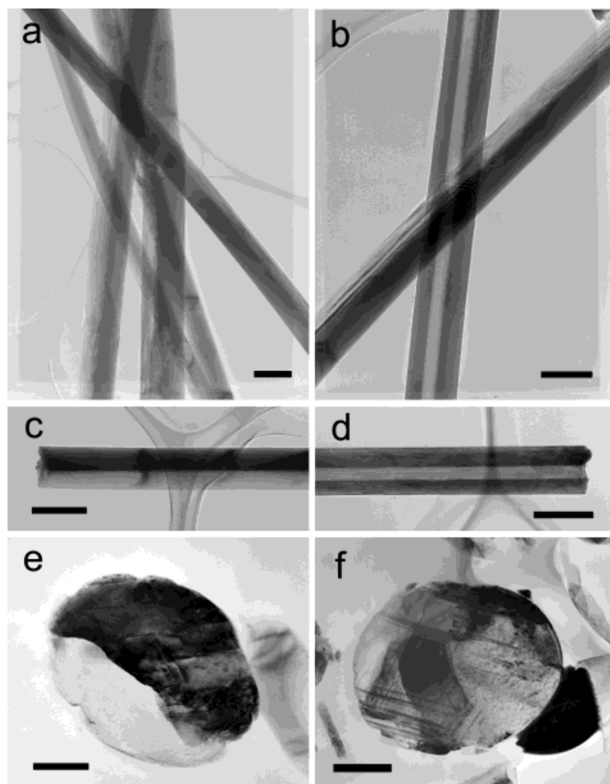

Figure 2. (a, b) Low-magnification TEM images of side-to-side Si−ZnS biaxial and sandwichlike ZnS−Si−ZnS triaxial nanowires, respectively. (c, d) Low-magnification TEM images of the tip-end characteristics of the side-to-side and sandwichlike nanowires, respectively. Scale bars in (a−d) are 100 nm. (e, f) Cross-sectional TEM images of side-to-side biaxial Si−ZnS and sandwichlike triaxial ZnS−Si−ZnS nanowires, respectively, Scale bars in (e, f): 30 nm.

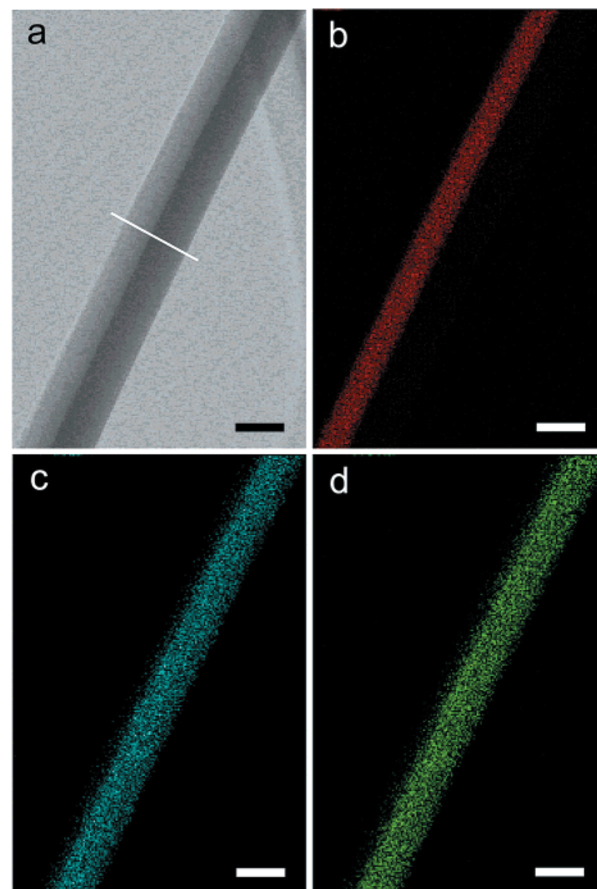

Figure 3. (a) High-magnification TEM image depicting a Si (light) and ZnS (dark) subnanowire sides within a Si−ZnS biaxial nanowire. (b−d) The Si, Zn, and S elemental mappings demonstrating a well-defined compositional profile and an abrupt interface. All scale bars in (a−d) are 50 nm.

with contrast variation unambiguously reveal the geometrical characteristics of the side-to-side biaxial Si−ZnS (Figure 2e) and the three-layer sandwichlike triaxial ZnS−Si−ZnS (Figure 2f) composite nanowires.

Examinations of the elemental mappings and EDS nanoanalysis (with probe size smaller than ∼1 nm) will shed light on the compositional homogeneity of these composite nanowire structures. Figure 3a shows a bright-field TEM image of a segment of a straight side-to-side Si−ZnS biaxial nanowire, which reveals a clear and uniform interface between the Si subnanowire (light) and ZnS subnanowire (dark), and the diameters of the subnanowires of Si and ZnS are ∼30 nm and ∼40 nm, respectively. The Si, Zn, and S elemental mappings from this composite nanowire (Figure 3b−d) further demonstrate that the biaxial Si−ZnS nanowire structure has a well-defined compositional profile and an abrupt interface (and external surface). An EDS spectrum in Figure 4a is recorded from the Si subnanowire within this biaxial Si−ZnS nanowire, which only reveals the presence of the Si peak (the C and the Cu signals come from a TEM grid), indicating the Si elemental composition of the Si subnanowire in the Si−ZnS biaxial nanowire. An EDS spectrum in Figure 4b is taken from the ZnS subnanowire side, which shows the presence of the Zn and S with an approximate stoichiometry of ZnS and with a very low content of Si, suggesting the main compositions of Zn and S in the ZnS subnanowire in the Si−ZnS composite nanowire. The spatial distributions of the atomic contents across the Si−ZnS biaxial nanowire are further obtained by a line-scanning (indicated by a line, Figure 3a) elemental mappings of Si, Zn, and S. The profile of Si shows a peak at the left side, while the profiles of Zn and S show peaks at the right side, directly featuring a side-to-side geometry of the Si−ZnS biaxial nanowire, which is different from the characteristics of the core−shell nanowire heterostructures.[13] Analysis of the data shows that the diameters of Si and ZnS subnanowires are ∼30 nm and ∼40 nm, respectively, which is consistent with the TEM image (Figure 3a), and the width of the Si−ZnS interface area is believed to be several nanometers. The profile of O possibly originates from the unavoidable surface-adsorption due to exposure to air during sample processing.

High-resolution TEM (HRTEM) images and ED patterns will reveal the structural homogeneity and an excellent epitaxial growth of the side-to-side Si−ZnS biaxial nanowire heterostructures. Parts a and b of Figure 5 are the HRTEM images of the Si and ZnS subnanowires within a Si−ZnS biaxial nanowire heterostructure, respectively, which are taken along the same electron beam direction without any sample tilting. It is worthwhile noting that either the Si-side or the ZnS-side displays the same imaging characteristics, which suggests that both subnanowires of Si and ZnS within this biaxial nanowire heterostructure have the same growth orientation. The marked interplanar *d* spacings (of ∼0.31 nm) correspond to that of the {111} lattice planes of the diamond-cubic Si and zinc blende ZnS, respectively. Being different from the reported biaxial

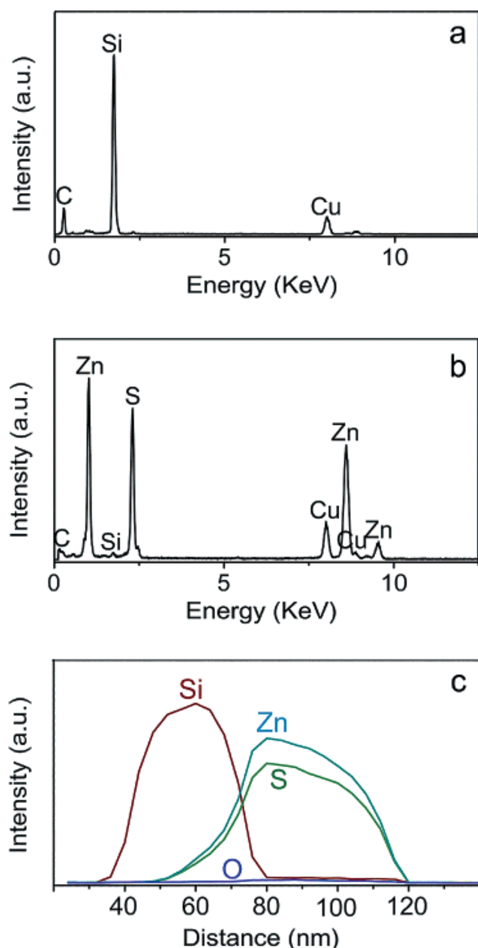

Figure 4. (a, b) EDS nanoanalysis spectra recorded from the sides of the Si and ZnS subnanowire, respectively. (c) Line-scanning (indicated by a line, Figure 3a) elemental mapping showing Si, Zn, and S elemental profiles across the Si−ZnS biaxial nanowires.

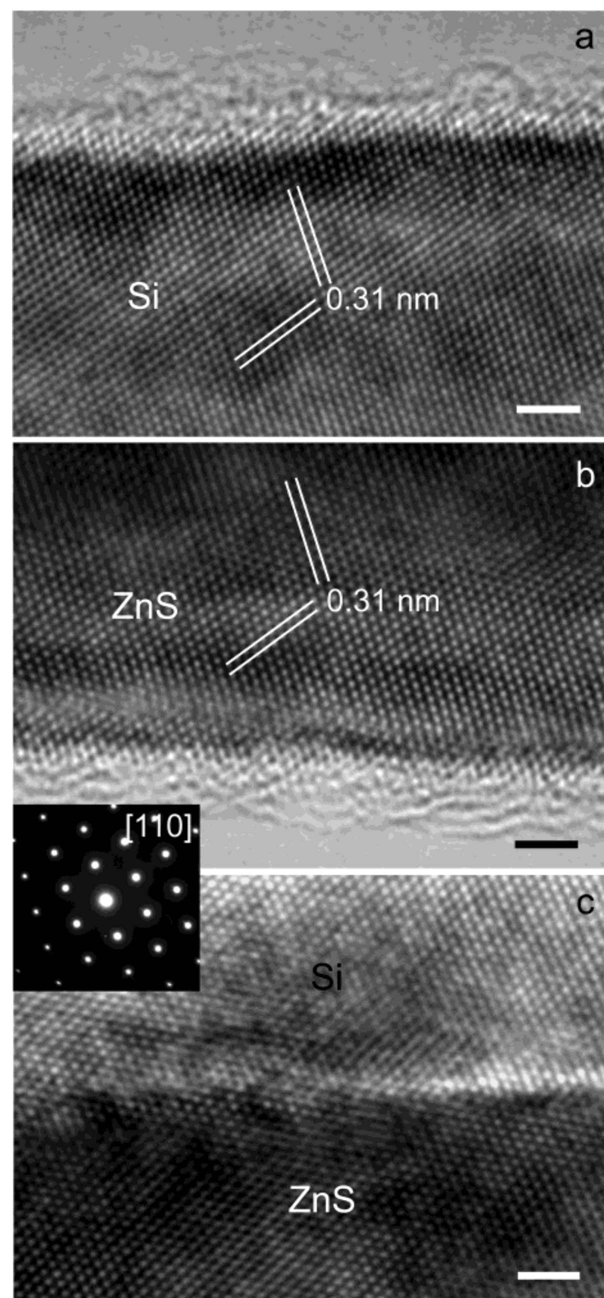

Figure 5. (a) HRTEM image of the Si subnanowire, two sets of {111} (d_{111} = 0.3135 nm) planes designated by double-lines. (b) HRTEM image of the ZnS subnanowire, two sets of {111} (d_{111} = 0.3123 nm) planes indicated by double-lines. (c) HRTEM image taken from the Si−ZnS interface domain, revealing a well-epitaxial relationship ($(111)_{Si}//(111)_{ZnS}$ and $(\bar{1}\bar{1}1)_{Si}//(\bar{1}\bar{1}1)_{ZnS}$) between the subnanowires of Si and ZnS. The ED pattern (upper left inset) taken from the interface area corresponding to the Si [110] zone axis or the ZnS [110] zone axis. All scale bars in (a−c) are 2 nm.

nanowires of SiC−SiO_2 (amorphous SiO_2),[25,26] the Si and ZnS subnanowires within a Si−ZnS biaxial nanowire heterostructure are both structurally uniform single crystals, and no dislocations or other planar defects are observed in them. In addition, it is further noticed that (even though the samples were exposed to air for several months) there are no amorphous sheathed phases attributed to oxidation observed on the surfaces commonly associated with Si nanowires.[19−21,27,28] A HRTEM image shown in Figure 5c is taken from the interface domain between the Si-side and ZnS-side. The interface is homogeneous and uniform at the atomic scale, and no amorphous layers attributed to silicon sulfides[29] are formed at it. An excellent epitaxial relationship between the Si-side and ZnS-side is clearly seen, and no misfit dislocations (the lattice mismatch of ∼0.40%) and no stress are observed at the interface in the HRTEM studies. The excellent epitaxy observed in these side-to-side biaxial Si−ZnS nanowires is very reasonable, considering the similar crystal structures and very close lattice constants of cubic Si and ZnS (ZnS: a = 0.5431 nm, Si: a = 0.5420 nm).[1] Extensive HRTEM imaging indicates that the homogeneity and well-epitaxial relationship of the Si−ZnS interface are maintained throughout its entire length. The Si−ZnS biaxial nanowires can grow with lengths ranging from several to several tens of micrometers, and thus, the coherent high-quantity interface region can be much more extended than that in the reported nanowire supperlattice heterostructures.[7−11] An ED pattern (Figure 5c, upper left inset) taken on the two sides of the Si−ZnS interface area corresponds

(25) Wang, Z. L.; Dai, Z. R.; Gao, R. P.; Bai, Z. G.; Gole, J. L. *Appl. Phys. Lett.* **2000**, *77*, 3349−3351.
(26) Sun, X. H.; Li, C. P.; Wong, W. K.; Wong, N. B.; Lee, C. S.; Lee, S. T.; Teo, B. K. *J. Am. Chem. Soc.* **2002**, *124*, 14464−14471.
(27) Morales A. M.; Lieber, C. M. *Science* **1998**, *279*, 208−211.
(28) Gole, J. L.; Stout, J. D.; Rauch, W. L.; Wang, Z. L. *Appl. Phys. Lett.* **2000**, *76*, 2346−2348.
(29) Weser, T.; Bogen, A.; Konard, B.; Schnell, R. D.; Schug, C. A.; Steinmann, W. In *Proceedings of the Eighteenth International Conference on the Physics of Semiconductors*, *Stockholm, Sweden, 1986*; Engström, O., Ed.; World Scientific: Singapore, 1987; pp 97−100.

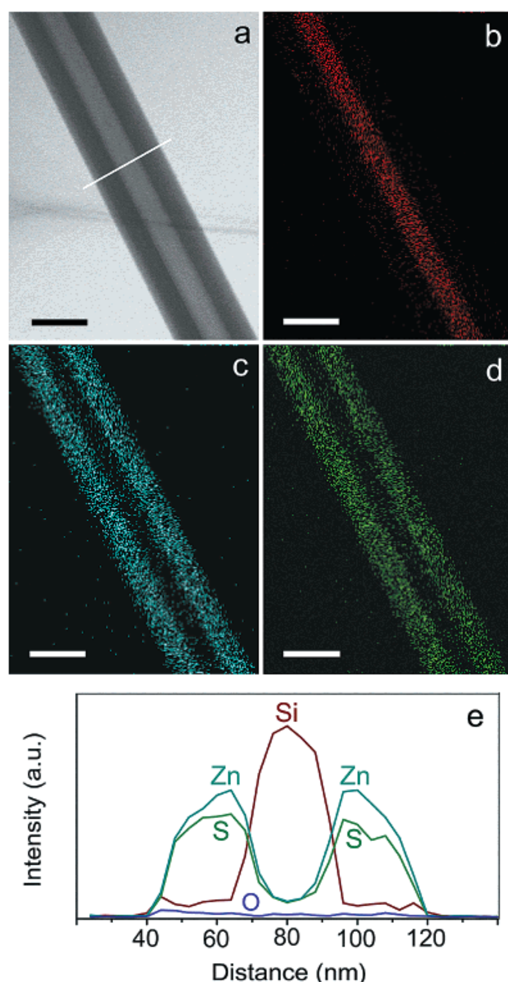

Figure 6. (a) High-magnification TEM image depicting two separated ZnS (dark) subnanowries and one central Si (light) subnanowire within a sandwichlike ZnS−Si−ZnS triaxial nanowire. (b−d) The Si, Zn, and S elemental mappings, respectively, directly revealing a three-layer sandwichlike geometry with well-defined compositional profiles. All scale bars in (a−d) are 50 nm. (e) Line-scanning (indicated by a line in a) elemental mapping of Si, Zn, and S elemental profiles across the sandwichlike ZnS−Si−ZnS triaxial nanowire.

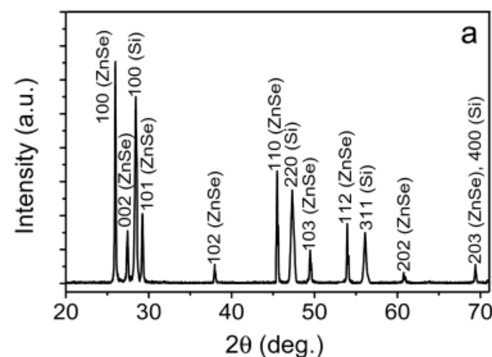

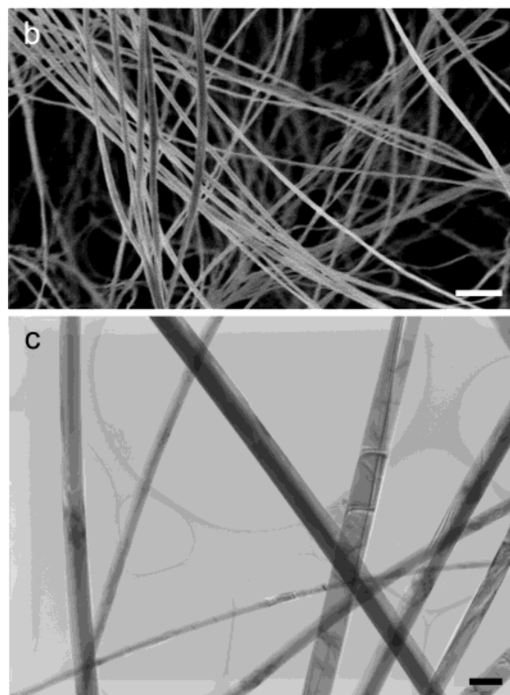

Figure 7. (a) A XRD pattern recorded from the product obtained from thermal evaporation of a mixed powder of SiO and ZnSe. (b) SEM image of the as-grown product. Scale bar: 1 μm. (c) Low-magnification TEM image of as-grown side-to-side Si−ZnSe biaxial nanowires. Scale bar: 100 nm.

to that of the Si [110] zone axis or the ZnS [110] zone axis. The excellent epitaxial relationship is established between the Si and ZnS, as revealed by the HRTEM image, i.e., $(111)_{Si}//(111)_{ZnS}$; $(\bar{1}\bar{1}1)_{Si}//(\bar{1}\bar{1}1)_{ZnS}$.

The sandwichlike ZnS−Si−ZnS triaxial nanowire heterostructures, which consist of two separated ZnS subnanowries and one central Si subnanowire, have also been achieved in the two-stage thermal evaporation of the mixed SiO and ZnS powders. Similarly to the Si−ZnS biaxial nanowire heterostructures, the sandwichlike ZnS−Si−ZnS triaxial nanowire heterostructures also display compositional and structural homogeneity, as well as excellent epitaxial relationships between the Si subnanowire and ZnS subnanowires throughout their entire lengths. Figure 6a shows a TEM image of a segment of a straight and long sandwichlike ZnS−Si−ZnS heterostructure, where the external surface and Si−ZnS interfaces are clean and uniform, and the central Si subnanowire (light) and the two separated ZnS subnanowires (dark) have a nearly equal diameter of 25−30 nm. The Si elemental mapping (Figure 6b) shows that Si is located at the center area along the longitudinal direction of the nanowire heterostructure. The Zn and S elemental mappings (Figure 6, c and d) display that Zn and S are both distributed at the left and right sides along the length with their absence in the center, directly revealing a three-layer sandwichlike nanowire structure with the well-defined compositional profiles. Elemental profiles across the ZnS−Si−ZnS nanowire heterostructure are also obtained through a line-scanning (indicated by a line, Figure 6a) elemental mapping. The profile of Si (Figure 6e) shows a peak at the center, while the profiles of Zn and S both show two peaks at the right and left sides with a gap in the center, which are quite different from the case of the side-to-side Si−ZnS biaxial nanowires, verifying a three-layer sandwiched (including two sides of ZnS subnanowires and one center of Si subnanowire) geometry of the ZnS−Si−ZnS nanowire heterostructure.

The similar two-stage temperature-controlled evaporation approach was used to grow side-to-side Si−ZnSe biaxial nanowires. The resulting yellow wirelike product was identified by XRD (Figure 7a) to be a composite material composed of cubic Si and hexagonal wurtzite ZnSe (JCPDS file: 15-0105). SEM observation (Figure 7b) shows that the as-grown product is composed of many wirelike nanostructures with typical

lengths of several tens of micrometers. A low-magnification TEM image (Figure 7c) reveals that the as-grown product also displays side-to-side biaxial nanowire structures, in which the lighter contrast side is pure Si subnanowire, and the darker contrast side is ZnSe subnanowire. Each side-to-side Si−ZnSe biaxial nanowire has a uniform diameter along the length, and the diameters are in the range of 40−90 nm. The diameters of Si and ZnSe subnanowires within these biaxial structures are ∼20−50 nm.

Figure 8a shows a high-magnification TEM image of a segment of a straight Si−ZnSe biaxial nanowire heterostructure, in which an interface between the subnanowires of Si (light) and ZnSe (dark) is clearly revealed. An ED (right lower inset, Figure 8a) pattern at the Si−ZnSe interface suggests only two sets of well-correlated diffraction spots, in which the spots marked with a rhombus corresponds to those from the Si $[1\bar{1}0]$ zone axis, whereas the other marked with a rectangle can be indexed as the wurtzite ZnSe [100] zone axis. In the ED pattern of the wurtzite ZnSe, the streaking along the c^* direction results from the stacking faults of the (010) planes, as suggested by the streaklike contrast on the observed faces in the TEM imaging. After further analysis of the ED pattern, an interfacial epitaxial relationship between the Si subnanowire and ZnSe subnanowire is also suggested, that is $(001)_{Si}//(010)_{ZnSe}$; $[001]_{Si}//[210]_{ZnSe}$. Parts b and c of Figure 8 show HRTEM images of the Si subnanowire and ZnSe subnanowire, respectively, which are taken along the same electron beam direction without any sample tilting. The marked interplanar d spacing (of ∼0.34 nm) corresponds to that of the (010) lattice plane of the hexagonal ZnSe (Figure 6b). Further HRTEM study indicates that the ZnSe subnanowire has a considerable density of stacking faults along its length, as revealed by the ED pattern, and the ZnSe subnanowire grows along the [210] crystallographic direction of the hexagonal wurtzite structure. In Figure 8c, the marked interplanar d spacing (of ∼0.31 nm) corresponds to those of the {111} lattice planes of the cubic Si. Being different from the ZnSe subnanowire, the Si subnanowire is structurally uniform and free of dislocations and other crystal defects throughout the entire length. Similar analysis shows that the Si subnanowire grows along [001] direction of the diamond-cubic structure. An HRTEM image shown in Figure 8d is taken from the interface domain between the Si- and ZnSe-side. In both of the above cases of the Si−ZnS biaxial nanowire and ZnS−Si−ZnS triaxial nanowire heterostructures, the Si−ZnS interfaces within them are clean and uniform at the atomic scale and no amorphous layers attributed to silicon sulfides are formed. However, in the case of the Si−ZnSe biaxial nanowire heterostructures, it can be seen that there is a thin (∼2 nm) intermediate layer at the Si−ZnSe interface between the Si subnanowire and ZnSe subnanowire, which is due to the reactivity of Si and Se and may give rise to the formation of disordered silicon selenium at the interface.[30,31] Extensive HRTEM imaging indicates that the intermediate layer of the disordered silicon selenium at the interface is maintained along its entire length.

EDS nanoanalysis and line-scanning elemental mappings will further confirm the compositional homogeneity in the Si−ZnSe biaxial nanowire heterostructures. The spectrum in Figure 9a is recorded from the Si subnanowire side, which reveals the

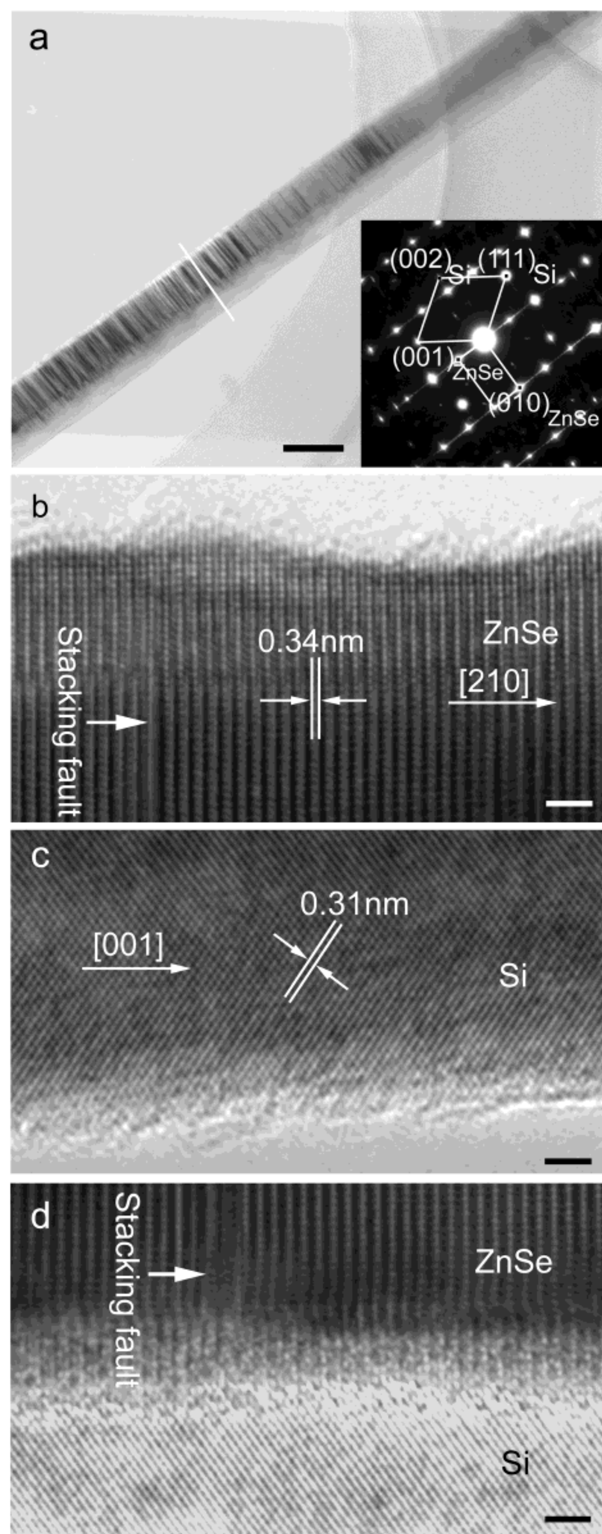

Figure 8. (a) High-magnification TEM image of a straight side-to-side Si−ZnSe biaxial nanowire. An ED pattern (upper left inset) taken from the Si−ZnSe interface area corresponding to the Si $[1\bar{1}0]$ zone axis or the ZnSe [100] zone axis, suggesting an epitaxial relationship (of $(001)_{Si}//(010)_{ZnSe}$ and $[001]_{Si}//[210]_{ZnSe}$) between the subnanowires of Si and ZnSe sides within it. Scale bar: 50 nm. (b) HRTEM image of the ZnSe subnanowire growing along [210] direction ($d_{010} = 0.34$ nm, as indicated by a double-line, stacking faults designed by an arrow). (c) HRTEM image of the Si subnanowire growing along [001] ($d_{111} = 0.31$ nm, as indicated by a double-line). (d) HRTEM image taken from a Si−ZnSe interface domain, revealing a thin intermediate layer between the Si and ZnSe subnanowires. All scale bars in (b−d) are 2 nm.

(30) Bringans, R. D.; Olmstead, M. A. *Phys. Rev. B* **1989**, *39*, 12985−12988.
(31) Bringans, R. D.; Biegelsen, D. K.; Swartz, L.-E.; Ponce, F. A.; Tramontana, J. C. *Phys. Rev. B* **1992**, *45*, 13400−13406.

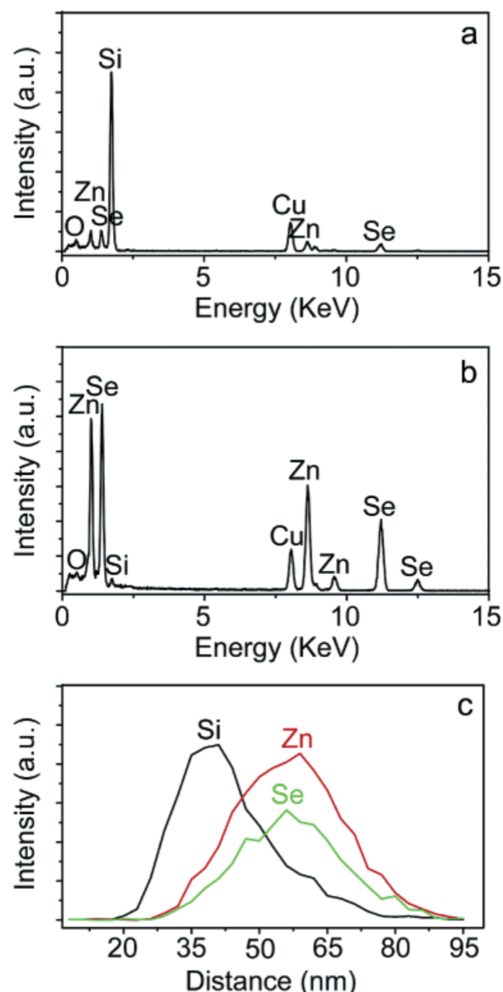

Figure 9. (a, b) EDS nanoanalysis spectra recorded from the sides of the Si and ZnSe subnanowire, respectively. (c) Line-scanning (indicated by a line, Figure 6a) elemental mapping showing Si, Zn, and Se elemental profiles across the Si–ZnSe biaxial nanowire.

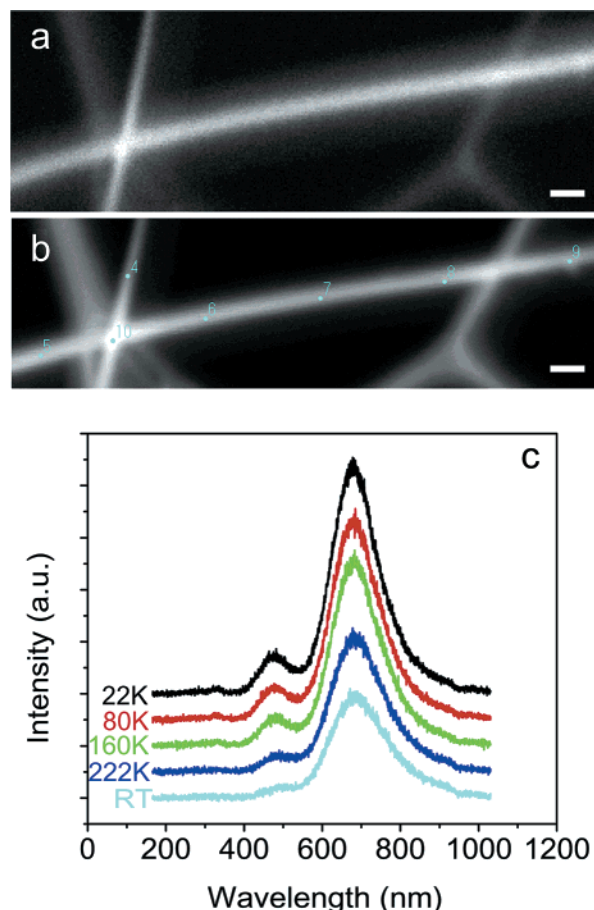

Figure 10. (a) CL image recorded at room temperature, an acceleration voltage of 5 kV, and a wavelength of 480 nm. (b) High-resolution TFE-SEM image from the same region. Scale bars in (a) and (b): 100 nm. (c) Nanoscale CL spectra revealing the temperature-dependent emission from Si and ZnS within a single side-to-side Si–ZnS nanowire heterostructure.

presence of Si, Zn, and Se (Cu signal comes from a TEM grid, and O signal possibly originates from the unavoidable surface-adsorption due to exposure to air during the processing of the sample.). Quantization of the spectrum shows that the amount (wt %) of Si is as high as 78.91 (85.35, at %), and the contents of Zn and Se are as low as 6.59 (3.06, at %) and 10.54 (4.05, at %), respectively, indicating the prime element Si of the Si subnanowire within the Si–ZnSe biaxial nanowire. The spectrum in Figure 9b is taken from the ZnSe subnanowire side, which indicates the presence of the Zn (46.11, wt %; 47.38, at %) and Se (51.28, wt %; 43.63, at %) with an approximate stoichiometry of ZnSe and with a very low content of Si (1.07, wt %; 2.56, at %), suggesting the main compositions of Zn and Se in the ZnSe subnanowire within the Si–ZnSe composite nanowire. The spatial distributions of the atomic contents across the Si–ZnSe nanowire heterostructure are further obtained by a line-scanning (indicated by a line, Figure 8a) elemental mappings of Si, Zn, and Se. The profile of Si shows a peak at the left side, while the profiles of Zn and Se show peaks at the right side, which is very similar to the characteristics of the Si–ZnS biaxial nanowire heterostructures, further revealing a side-to-side geometry of the Si–ZnSe biaxial nanowires with compositional modulation profiles (The Si, Zn, and Se elemental mappings also demonstrate the side-to-side geometric characteristic of the Si–ZnSe biaxial nanowires (See Supporting Information)). Analysis of the data shows that the subnanowires of Si- and ZnSe-side within it are ~30 nm in diameter, and the intermediate layer of silicon selenium at the interface is estimated to be several nanometers in thickness.

To investigate the optical properties of individual side-to-side Si–ZnS and Si–ZnSe biaxial nanowires, and ZnS–Si–ZnS triaxial nanowires, we carried out the nanoscale cathodoluminescence (and imaging) and further studied the temperature-dependent emission from Si, ZnS, or ZnSe subnanowire within a single composite nanostructure. To visualize the spatial distribution of the luminescence from a single Si–ZnS biaxial nanowire, a CL image was recorded at room temperature and at a wavelength of 480 nm, as shown in Figure 10a. By taking a TFE-SEM image from the same region, (Figure 10b) the luminescence and the structure of the Si–ZnS biaxial nanowire could be obtained. Figure 10c shows CL spectra of an individual Si–ZnS biaxial nanowire at five different temperatures of 22, 80, 160, 222, and 299 K (room temperature). The CL spectra are basically composed of two peaks. A strong peak at ~680 nm (~1.82 eV) is visible emission from the Si subnanowire, which is comparable to the best values for bulk Si nanowires.[32] A weak and broad peak centered at ~476 nm (~2.60 eV) is

(32) Zhang, Y. F.; Tang, Y. H.; Peng, H. Y.; Wang, N.; Lee, C. S.; Bello, I.; Lee, S. T. *Appl. Phys. Lett.* **1999**, *75*, 1842–1844.

visible (blue) emission related to some defects within the ZnS subnanowire, which are peculiar to bulk ZnS nanowires.[33,34] At $T = 22$ and 80 K, a very weak peak at ~330 nm (~3.75 eV) is a UV emission attributed to the band edge luminescence of ZnS. With increasing temperature, the intensities and line widths of these emission peaks gradually became weaker and broader. We also performed a CL line-scan from one end to the other of an individual Si−ZnS nanowire heterostructure, and almost the same emission was observed. In the case of individual sandwichlike ZnS−Si−ZnS nanowire heterostructures, these emission peaks are the same with the exception of the increase of the CL intensity. The cathodoluminescence and imaging of the Si−ZnSe biaxial nanowires are available in Supporting Information.

The growth of the novel nanostructures discussed above was accomplished by simple thermal evaporation of a mixed powder of SiO and ZnS or SiO and ZnSe via a two-stage process under careful temperature control. In the first evaporation stage, condensation of a Si vapor due to disproportionation of SiO to Si + SiO_2 led to the growth of Si nanowires.[19−21] In the present case, the reduction atmosphere from the high-purity graphite (induction-heated cylinder) at high temperature will be important to as-grown Si nanowires because the Si nanowires can resist significant oxidation in such a reduction atmosphere at the processing temperature; otherwise the surface of the Si nanowires will be oxidized and results in the formation of Si/SiO_2 core−shell nanostructures.[19−21,27,28] The as-formed Si nanowires exhibit surface dangling bonds or surface dimmer bonds or both,[35] and the surfaces of the Si nanowires are energetically favorable. Thus, these Si nanowires can be used as one-dimensional substrates for conceivable vapor deposition processes. In the second evaporation stage, the adsorption or deposition of ZnS or ZnSe vapor will occur at the surfaces of these Si nanowire one-dimensional substrates. The nucleation of ZnS or ZnSe crystallites takes place epitaxially on the surfaces of Si nanowire substrates, as demonstrated in the epitaxial growth of ZnS or ZnSe thin films on Si substrates.[36−41] The lattice rearrangement (from the diamond-cubic Si to zinc blende cubic ZnS or to hexagonal wurtzite ZnSe) easily occurs at the Si nanowire surface front, in particular, at the terraces having surface dangling bonds. The ZnS (or ZnSe) crystallites will grow on their lowest-energy faces {111} (or {010}), parallel to those of the Si nanowires, forming the well-epitaxial relationship between the subnanowires of Si and ZnS or Si and ZnSe. In most cases, the Si nanowires formed lie on the C fiber thermo-insulting layer. Usually, there is only one side plane of a given Si nanowire open to the environment. The exposed side plane of Si nanowires will be coated when the ZnS or ZnSe vapor is deposited, leading to the formation of two sides characteristic of Si−ZnS or Si−ZnSe biaxial nanowires, which are similar to the case of SnO_2 nanoribbons as substrates for the growth of composite bilayer nanotaps.[12] In other cases, the formed Si nanowires could be free-standing on the C fiber thermo-insulting layer and have alternative side planes exposed to the environment for the growth of the two ZnS subnanowire thin layers on them. This may explain the formation of the sandwichlike ZnS−Si−ZnS triaxial nanowire heterostructures.

Conclusions

Epitaxial semiconducting heterostructures (side-to-side Si−ZnS, Si−ZnSe biaxial nanowires and sandwichlike ZnS−Si−ZnS triaxial nanowires) have been achieved via a simple two-stage thermal evaporation of the mixed SiO and ZnSe or SiO and ZnSe powders under a precise temperature control. Each nanowire had a uniform diameter of 40−120 nm and lengths ranging from several to several tens of micrometers. The subnanowires of Si-, ZnS, and ZnSe-side within them had a diameter of 20−50, 40−60, and 20−50 nm, respectively. High-quality epitaxial heterostructures of Si−ZnS, Si−ZnSe biaxial nanowires, and ZnS−Si−ZnS triaxial nanowires differ significantly from previously reposted core−sheath nanostructures.[13] Importantly, the large band-gap difference (Si: a band gap of 1.12 eV) between the two different semiconductors should make Si-based optoelectronic nanodevices and the integration of ZnS- or ZnSe-based nanodevices with Si-integrated circuits possible. Although the detailed growth mechanism requires more systematic investigations, the present results suggest that the simple method might be useful for the synthesis of many other composite nanowires containing Si and II−VI or III−V semiconductors to meet the growing demands of nanoscale science and technology.

Acknowledgment. This work was supported by the Japan Society for the Promotion of Science (JSPS) Fellowship at the National Institute for Materials Science, Tsukuba, Japan.

Supporting Information Available: Si, Zn, and Se elemental mappings and cathodoluminescence and imaging of the Si−ZnSe biaxial nanowires (PDF). This material is available free of charge via the Internet at http://pubs.acs.org.

JA030235L

(33) Jiang, X. C.; Xie, Y.; Lu, J.; Zhu, L. Y.; He, W.; Qian, Y. T. *Chem. Mater.* **2001**, *13*, 1213−1218.
(34) Wang, X. D.; Gao, P. X.; Li, J.; Summers, C. J.; Wang, Z. L. *Adv. Mater.* **2002**, *14*, 1732−1735.
(35) Zhang, R. Q.; Lee, S. T.; Law, C.-K.; Li, W.-K.; Teo, B. K.*Chem. Phys. Lett.* **2002**, *364*, 251−258.
(36) Romano, L. T.; Bringans, R. D.; Zhou, X.; Kirk, W. P. *Phys. Rev. B.* **1995**, *52*, 11201−11205.
(37) Zhou, X.; Jiang, S.; Kirk, W. P. *J. Appl. Phys.* **1997**, *82*, 2251−2262.
(38) Tran, N. H.; Hartmann, A. J.; Lamb, R. N. *J. Phys. Chem. B* **2000**, *104*, 1150−1152.
(39) Chern, M. Y.; Lin, H. M.; Fang, C. C.; Fan, J. C.; Chen, Y. F. *Appl. Phys. Lett.* **1995**, *67*, 1390−1392.
(40) Miwa, S.; Kuo, L. H.; Kimura, K.; Ohtake, A.; Yasuda, T.; Jin, C. G.; Yao, T. *Appl. Phys. Lett.* **1997**, *71*, 1192−1194.
(41) Romano, L. T.; Bringans, R. D.; Zhou, X.; Kirk, W. P. *Phys. Rev. B* **1995**, *52*, 11201−11205.